RDQI = 3: The quality of the pixel is scientifically and cosmetically unusable. In addition, the shielded pixels at the end of each line array are marked with an RDQI of 3.

During laboratory calibration, a "gain" is computed from the slope of camera output DN to total-band incident radiance, *I*. It is observed that pixels with a large out-of-band leakage have a larger uncertainty in this gain, in that it is observed to vary with the spectrum of the incident light. A data quality indicator can thus be computed based on the change in gain with different illumination sources. Specifically, we take the ratio of the gain computed with an incandescent lamp to the gain computed from adding a UV plasma lamp. Pixels for which this gain ratio is between 0.95 and 1.05 are assigned an RDQI value of 0 indicating that out-of-band light is a small contributor to the measured radiance. Pixels for which the gain ratio is outside of this range, but between 0.90 and 1.10 are assigned an RDQI value of 1. Pixels with gain ratios outside both these ranges, but between 0.80 and 1.20 are assigned an RDQI value of 2. All other pixels are assigned an RDQI value of 3. The observed out-of-band leakage is believed to be the cause of permanent striping in the images, which is particularly noticeable in the UV bands.

Pixels marked with RDQI = 0 are expected to have an absolute radiometric uncertainty of ~5% (1σ). This radiometric uncertainty is attributed to the vicarious calibration methodology, which sets the absolute radiometric scale. The laboratory calibration is used to establish the relative-pixel response, also known as "flat-fielding". Comparisons of radiometric laboratory calibrations before (30 March 2016) and after (19 January 2017) ORACLES suggest that the sensor remained stable during the campaign, so while the vicarious calibration is being performed it was decided to provide the AirMSPI data with only the laboratory calibration applied as an initial data release.

3 SPECTRAL CALIBRATION

Determination of the detailed spectral response function (SRF) of each AirMSPI channel has been made based on the laboratory calibration of 9 December 2013. A monochromator was used for this purpose. The SRF is equal to the camera response to monochromatic light normalized by a silicon diode response. The monochromator provided wavelength scans from 300 to 2500 nm. Two sources were used in separate spectral scans of all channels — a Luxim Light Emitting Plasma lamp for ultraviolet-blue, and a quartz-halogen lamp for the remaining visible and near-infrared channels. The results of this calibration are shown in Table 1 and Figure 2.

In the current product release (V006), center wavelengths, effective (equivalent square-band) bandwidths, and effective (equivalent square-band) transmittances are calculated by applying the moments method of Palmer (1984) to the normalized spectral response of each band over the range 300-1100 nm. Solar irradiances are weighted by the total-band spectral response. The Wehrli (1985) extraterrestrial solar spectrum was used for this purpose. These values are provided in Table 1 below, and represent the total-band response.

In general, radiometric response at wavelengths far from the "in-band" spectral region is estimated at $< 10^{-4}$ of the peak response, though as noted above, a larger amount of out-of-band leakage is present in a small subset of pixels in the UV bands, leading to striping in a portion of

the UV images. Currently uncorrected striping in the 355 and 380 nm bands is attributed to filter blemishes that create a scene-dependent scattered light response.

Table 1 – Total-band effective center wavelength, bandwidth and transmittance, and total-band weighted solar irradiance E_0 [W m^{-2} nm^{-1}] at 1 AU

Channel Name	Center Wavelength (nm)	Effective Bandwidth (nm)	Effective Transmittance	Solar Irradiance (W m^{-2} nm^{-1})
355I	355.1	47.7	0.609	1.002
380I	377.2	40.4	0.750	1.079
445I	443.3	46.0	0.799	1.861
470I	469.1	45.5	0.824	2.000
470Q	469.4	45.0	0.837	1.999
470U	468.8	46.0	0.815	2.000
555I	553.5	38.6	0.758	1.857
660I	659.2	45.2	0.835	1.555
660Q	659.1	43.8	0.881	1.556
660U	659.1	48.2	0.798	1.556
865I	863.3	43.5	0.829	0.976
865Q	863.7	45.6	0.810	0.976
865U	864.1	48.5	0.753	0.975
935I	931.3	53.2	0.809	0.823

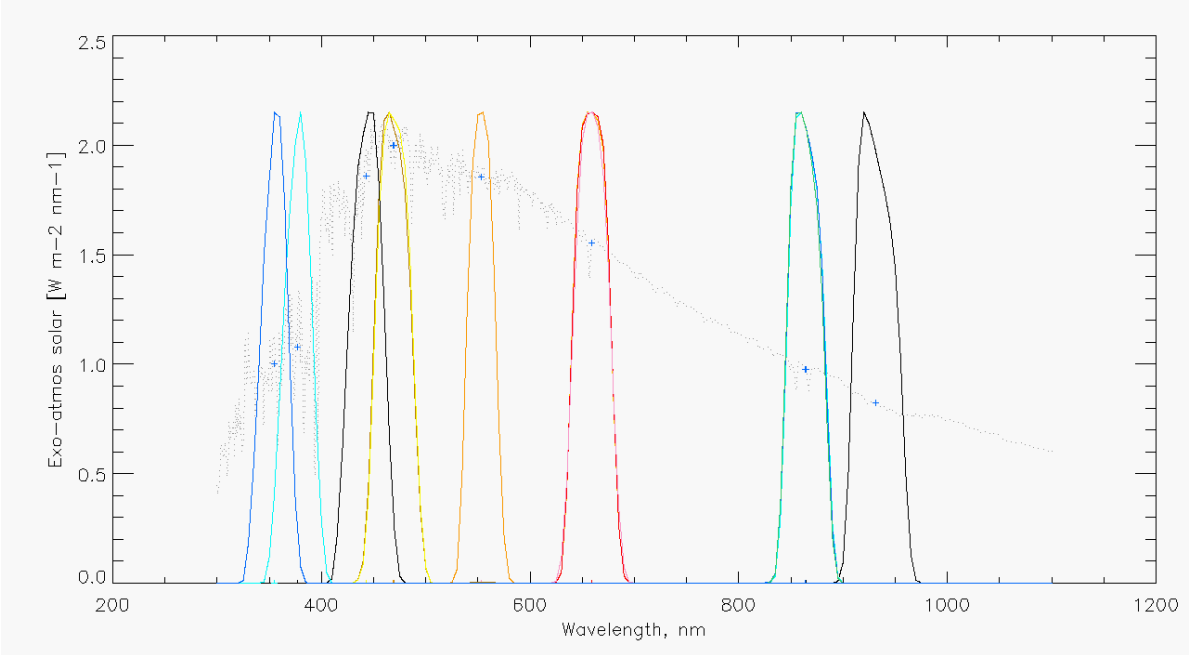

Figure 2. AirMSPI spectral response functions (SRF) shown in colored lines with the Wehrli (1985) exoatmospheric solar irradiance values shown in the faint, gray, dotted line. E0 values at 1 AU are indicated by the "+" symbol.

4 POLARIMETRIC CALIBRATION

AirMSPI uses a time-varying retardance in the optical path to modulate the orientation of the linearly polarized component of the incoming light, described by the Stokes components Q (excess of horizontally over vertically polarized light) and U (excess of 45º over 135º polarized light) (Diner et al., 2007, 2010; Mahler et al., 2011). As a result, the ratios of these parameters to the radiance I, given by $q = Q/I$ and $u = U/I$ are to first order insensitive to the absolute radiometric calibration of a given pixel because both the numerator and denominator are determined from signals acquired by the same detector element. The degree of linear polarization (DOLP) and angle of linear polarization (AOLP) derived from these ratios, equal to $\sqrt{q^2 + u^2}$ and $0.5\tan^{-1}(u/q)$, respectively, are likewise insensitive to absolute radiometric calibration, based on similar considerations. To compensate for instrumental polarization aberrations (e.g., mirror diattenuation, imperfect retardance), a set of 10 polarimetric calibration coefficients is established for every pixel (Diner et al., 2010).

Two specialized pieces of equipment exist for verifying and controlling the performance of the polarimetric measurement approach during in-flight operations of AirMSPI. The first is an optical probe, which continuously sends a beam of light through the PEMs to monitor their retardances and phases. The information from the probe shows how far the PEM retardances and phases are from their desired values. A feedback control system within the instrument then adjusts the PEM parameters to drive the error signals to zero. Test data demonstrated the ability to control the PEM retardance and phase parameters to within a fraction of 1 mrad, keeping contributions to the overall DOLP uncertainty budget at <0.001. The second polarization monitoring system is an external polarization validator, which consists of nine light-emitting diodes (LEDs), three each at the AirMSPI polarimetric bands, that illuminate a plastic diffuser. In front of the diffuser, sheet polarizers are placed in different orientations. The validator is viewed before and after every multiangle observation of an Earth scene. Information from the validator system is used to derive instrument dark current and evaluate the stability of the DOLP measurements.

Results from a ground-based version of the instrument, GroundMSPI (Diner et al., 2012), show systematic DOLP uncertainties (excluding the effects of random noise), determined as the root-mean-square residual in DOLP as a polarizer is rotated in front of the camera, of ±0.003 or better. Results for AirMSPI, using the rotating polarizer methodology described in Diner et al. (2010), show similar residuals.

5 GEORECTIFICATION AND CO-REGISTRATION

As a part of the ground data processing, AirMSPI data from all spectral bands and all viewing angles are georectified and co-registered to a common Earth-based, Universal Transverse Mercator (UTM) projection grid. Distortions that can be associated with AirMSPI's type of pushbroom remote sensing imaging are taken into account by properly defining instantaneous pixel projection rays using ancillary data such as estimates of camera internal viewing geometry and ER-2 navigation data, which provide dynamic measures of the platform altitude and attitude variations. There are two types of AirMSPI georectified data products: 1) terrain projected and 2) ellipsoid projected. Terrain-projected data use a digital elevation model (DEM) for the projection

surface so that cloud-free imagery is truly orthorectified with reference to that surface. Ellipsoid-projected data use the World Geodetic System 1984 (WGS84) Earth reference ellipsoid for the projection surface. For this release, only the terrain-projected data are available with both ellipsoid- and terrain-projected data expected to be provided in the next data release.

Factors affecting geospatial accuracy of AirMSPI products include: 1) relative band-to-band co-registration within a single viewing angle, 2) multi-angle co-registration, and 3) absolute georectification. The uncertainty depends on the magnitude of the errors in the supplied ancillary data and errors in the projection surface defined by the DEM. For data sets acquired over land a terrain-projected data product is also derived based on a JPL internal version of the Shuttle Radar Topography Mission (SRTM) Plus (SRTMv3 60n-60s; ASTERv2 60n-83s; RAMP 60s-90s; JPL-LRR020977) with 30 m horizontal postings. Errors in the ancillary data defining viewing geometry are handled as static and dynamic pointing errors in order to characterize them using available ground control points (GCPs) in a procedure based on simultaneous bundle adjustment (Jovanovic et al., 2012). For targets where there is an optimum number of GCPs available, both static and dynamic pointing errors are recovered simultaneously prior to georectification and co-registration. These data are denoted as having full geometric calibration “directly” applied with expected co-registration and georectification uncertainty of around 15 m rms across all viewing angles and all bands. For other targets, (i.e., those without available GCPs, which are mostly fully ocean or cloudy imagery), an estimate of static pointing errors made on separate flight lines within the same campaign is utilized. These products are denoted as having geometric calibration “indirectly” applied with a current estimate of georectification and co-registration uncertainty of less than one hundred meters. The type of geometric calibration is recorded in the file metadata list under the field name “Geolocation stage”. Analysis and implementation efforts are still in progress with an objective to fully optimize the camera viewing model so that uncertainties of indirectly calibrated data are minimized.

Band-to-band relative co-registration uncertainty within the same viewing angle is well within 10 m, which is the pixel size of the map projection grid in the step-and-stare terrain-projected data. In the case of ellipsoid-projected data there will be some offsets in the relative band-to-band registration due to the parallax caused by the true height of the viewing surface and physical band separation in the focal plane. Additionally, slight errors in registration can cause a small displacement (on the order of a degree or two) of polarimetric features such as the backscatter glory from their expected location.

6 REFERENCES

Diner, D.J., A. Davis, B. Hancock, G. Gutt, R.A. Chipman, and B. Cairns (2007). Dual photoelastic modulator-based polarimetric imaging concept for aerosol remote sensing. *Appl. Opt.* **46**, 8428-8445.

Diner, D.J., A. Davis, B. Hancock, S. Geier, B. Rheingans, V. Jovanovic, M. Bull, D.M. Rider, R.A. Chipman, A. Mahler, and S.C. McClain (2010). First results from a dual photoelastic modulator-based polarimetric camera. *Appl. Opt.* **49**, 2929-2946.

Diner, D.J., F. Xu, J.V. Martonchik, B.E. Rheingans, S. Geier, V.M. Jovanovic, A. Davis, R.A. Chipman, and S.C. and McClain (2012). Exploration of a polarized surface bidirectional reflectance model using the Ground-based Multiangle SpectroPolarimetric Imager. *Atmosphere* **3**, 591-619.

Diner, D.J., F. Xu, M.J. Garay, J.V. Martonchik, B.E. Rheingans, S. Geier, A. Davis, B.R. Hancock, V.M. Jovanovic, M.A. Bull, K. Capraro, R.A. Chipman, and S.C. McClain (2013a). The Airborne Multiangle SpectroPolarimetric Imager (AirMSPI): a new tool for aerosol and cloud remote sensing. *Atmos. Meas. Tech*. **6**, 2007-2025.

Diner, D.J., M.J. Garay, O.V. Kalashnikova, B.E. Rheingans, S. Geier, M.A. Bull, V.M. Jovanovic, F. Xu, C.J. Bruegge, A. Davis, K. Crabtree, and R.A. Chipman (2013b). Airborne Multiangle SpectroPolarmetric Imager (AirMSPI) observations over California during NASA's Polarimeter Definition Experiment (PODEX). *SPIE Proc*. **8873**, 88730B-2.

Jovanovic, V.M., M. Bull, D.J. Diner, S. Geier, and B. Rheingans (2012). Automated data production for a novel Airborne Multiangle SpectroPolarimetric Imager (AirMSPI). *Int. Arch. Photogramm. Remote Sens. Spatial Inf. Sci.*, **XXXIX-B1**, 33-38.

Mahler, A., D.J. Diner, and R.A. Chipman (2011). Analysis of static and time-varying polarization errors in the multiangle spectropolarimetric imager. *Appl. Opt.* **50**, 2080-2087.

Palmer, J.M. (1984). Effective bandwidths for LANDSAT-4 and LANDSAT-D' Multispectral Scanner and Thematic Mapper subsystems. *IEEE Trans. Geosci. Rem. Sens.* **GE-22**, 336-338.

Wehrli, C. (1985). "Extraterrestrial Solar Spectrum", Publication no. 615, Physikalisch Meteorologisches Observatorium + World Radiation Center (PMO/WRC) Davos Dorf, Switzerland, July 1985.

Xu, F., A.B. Davis, R.A. West, and L.W. Esposito (2010). Markov chain formalism for polarized light transfer in plane-parallel atmospheres, with numerical comparison to the Monte Carlo method, *Opt. Express* **19**, 946-967.

7 APPENDIX A

Acronym List:

AFRC	Armstrong Flight Research Center
AirMSPI	Airborne Multiangle SpectroPolarimetric Imager
AOLP	Angle of Linear Polarization
ASD	Analytical Spectral Devices
ASDC	Atmospheric Science Data Center
AVIRIS	Airborne Visible/Infrared Imaging Spectrometer
AU	Astronomical Unit
DEM	Digital Elevation Model
DN	Digital Number
DOLP	Degree of Linear Polarization
EOS	Earth Observing System
FIREX-AQ	Fire Influence on Regional to Global Environments and Air Quality
GCP	Ground Control Point
HDF-EOS	Hierarchical Data Format for EOS
JPL	Jet Propulsion Laboratory
LaRC	Langley Research Center (NASA)
LED	Light Emitting Diode
MISR	Multi-angle Imaging SpectroRadiometer
NASA	National Aeronautics and Space Administration
NED	National Elevation Dataset
NIST	National Institute of Standards and Technology
NOAA	National Oceanic and Atmospheric Administration
RDQI	Radiometric Data Quality Indicator
SCF	Science Computing Facility
SDP	Science Data Processing
SI	*Système international*
SRF	Spectral Response Function
SRTM	Shuttle Radar Topography Mission
USGS	United States Geological Survey
UTM	Universal Transverse Mercator
UV	Ultraviolet
WGS84	World Geodetic System 1984